J. Fluid Mech. (2003), *vol.* 480, *pp.* 43–60.
DOI: 10.1017/S0022112003003732 Printed in the United Kingdom

Cavitation luminescence from flow over a hydrofoil in a cavitation tunnel

By T. G. LEIGHTON[1]†, M. FARHAT[2], J. E. FIELD[1]‡ AND F. AVELLAN[2]

[1]Cavendish Laboratory, Madingley Road, Cambridge, CB3 0HE, UK

[2]Institut de Machines Hydrauliques et de Mécanique des Fluides, École Polytechnique Fédérale de Lausanne (EPFL), 33, Av. de Cour, Lausanne, Switzerland

(Received 23 February 2001 and in revised form 5 September 2002)

This paper describes a photon-counting study of the cavitation luminescence produced by flow over a hydrofoil. This has previously been identified in water saturated with xenon. The four objectives of this study are: to determine whether luminescence can be obtained using air-saturated water; to quantify this emission, if it is present, as a function of flow parameters; to determine whether the photon arrivals occur with random timing, or in 'bursts'; to put limits on the rates associated with any bursts. The flow experiments were performed in a cavitation tunnel capable of achieving flow velocities of up to about $50\,\mathrm{m\,s^{-1}}$ in the test section. The experimental hydrofoil was a NACA 009 blade. Parameters varied were the flow velocity, the incident angle of the hydrofoil and the cavitation index. The results show that significant photon counts are recorded when leading-edge cavitation takes place and U-shaped vortices (cavities) are shed from the main cavity. The photon count increases dramatically as the flow velocity increases or the cavitation index is reduced. Departures from a Poisson distribution in the arrival times of photons at the detector suggest the presence of 'bursts'. These may be related to the way vortices are shed from the main cavity. Limits are inferred on the detection rates associated with bursts.

1. Introduction

The development of leading-edge cavitation on a hydrofoil is a potentially dangerous erosion situation; see, for example, Karimi & Avellan (1986). This type of cavitation is usually encountered on hydraulic runners and is characterized by the formation of a vapour cavity attached to the leading edge of the blades. This main cavity sheds vapour cavities, entrained within vortices in the liquid (Avellan & Karimi 1987; Avellan, Dupont & Farhat 1991; Arndt 2002). These transient features are convected by the flow and collapse violently in the pressure recovery region. The resulting overpressure may reach up to 2 GPa (Avellan & Farhat 1989). Cavitation erosion is caused by these repeated collapses. Such cavitation also gives rise to a number of other effects, notably acoustic emissions, which include pressure waves generated when the cavities collapse. The emission can be generated from rebound shocks or through liquid jet impact if the bubble involutes during collapse.

† Present address: Institute of Sound and Vibration Research (ISVR), University of Southampton, SO17 1BJ, UK.

‡ Author to whom correspondence should be addressed.

Type of flow	Angle of attack, α (deg.)	n (noise)	m (luminescence)
(i) Bubble	2	0.9	−1.8
	2° (no Xe)	0.7	–
(ii) Sheet	4	5.9	7.2
(iii) Sheet cloud	7	5.1	6.5
(iv) Vortex cloud	11	4.8	3.9

TABLE 1. Velocity exponents (dimensionless) relating to noise and luminescence (after van der Meulen 1986*b*).

In addition to these, cavitation can also cause luminescent emissions. Although, as Walton & Reynolds (1984) point out, the term 'cavitation luminescence' would be a better description for emissions that result from the cavitation generated by hydrodynamic flow, liquid impact, laser and spark discharge, and the collapse of vacuums, colloquially these are often termed 'sonoluminescence'. This imprecise nomenclature arose from acoustics being mainly used to generate the cavitation in the early decades (Marinesco & Trillat 1933; Jarman 1960; Knapp, Daily & Hammett 1970). The current debate on the commonality of the sources of the various luminescences calls this nomenclature into question (Barber *et al.* 1992; Matula & Roy 1997; Blake 1999; Leighton, Cox & Phelps 2000; Hammer & Frommhold 2001).

Compared with the prevalence of acoustic systems, there are few studies on the cavitation luminescence generated by hydrodynamic flow (Peterson 1966, 1967; van der Meulen 1983, 1986*a*, *b*; van der Meulen & Nakashima 1983). Van der Meulen used a high-speed flow tunnel with a NACA 16-022 hydrofoil set at various angles. By changing the angle of attack of the blade, α, and the upstream velocity C_{ref}, he produced four regimes of flow which he termed (i) bubble, (ii) sheet, (iii) sheet-cloud, and (iv) vortex-cloud cavitation. These regimes were studied photographically and both noise and luminescence measurements made.

In all his studies, van der Meulen was unable to detect any luminescence from 'undoped' water, but with the addition of xenon (to a dissolved concentration of typically $18\,\mathrm{ml\,l^{-1}}$, a well-established procedure for enhancing cavitation luminescence) the luminescence was detectable by the unaided eye. It was not quantified in the 1983 studies, but rather photographed (30 minute exposures are published). The 1983 studies used only $C_{ref} = 15\,\mathrm{m\,s^{-1}}$. Interestingly, with the naked eye 'bright flashes could be observed occasionally, in addition to the more or less continuous light emission' (for a 3 cm cavity length and $\alpha = 10°$). For $\alpha = 7°$, they denote that whilst luminescence was bright and constant from 25–55% of the way along the chord, from 50–90% along the chord "bright flashes could be observed frequently" (van der Meulen & Nakashima 1983). No further quantification of timescales or light output is given.

In the 1986 studies, van der Meulen did use photomultiplication. He found that the 'maximum luminous intensity' varied as C_{ref}^m where $-1.8 < m < 7.2$; and the broadband sound pressure level varied as C_{ref}^n where $4.8 < n < 5.9$. Note that only one of the set of conditions tested ($\alpha = 2°$; $C_{ref} = 10$–$20\,\mathrm{m\,s^{-1}}$) gave a negative value for m (i.e. luminous intensity decreased with increasing velocity). Considering the complexity of the measurements, the agreement between n and m for the flow types (ii) and (iv) is important. Van der Meulen's 1986 data are summarized in table 1. Van der Meulen (1986*b*) concluded that his research had established a useful link between

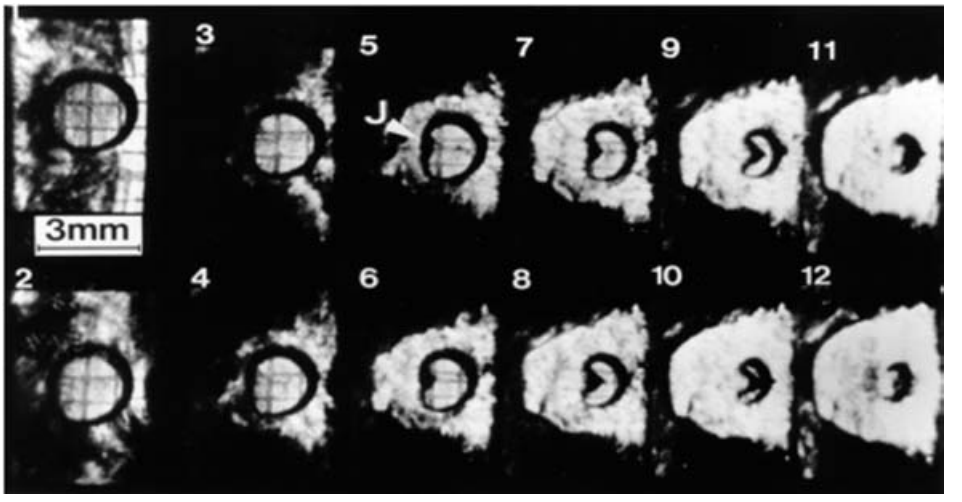

FIGURE 1. Two-dimensional cavity, diameter 3 mm, collapsed by a shock wave travelling left to right. The rear surface involutes to produce a jet, J, of about 400 m s^{-1}. Interframe time 0.96 μs. (After Dear *et al.* 1988.)

erosion (measured in the 1983 studies by monitoring 'pitting'), noise generation and luminescence.

Though pioneering in such comparisons, and in the use of a slit/lens system to measure the luminescence from a movable small region measuring 1.4 mm along the chord and 3.1 mm across the span, the quantification of the luminescence is rudimentary. Van der Meulen states that "no attempt was made to measure the absolute light intensity...only relative light intensities were measured by a pulse counter". The inability to detect luminescence unless the water had been first degassed and then doped with xenon indicates a sensitivity/signal-to-noise problem, and limits the practicality and cost-effectiveness of the technique. Rectifying these two limitations is technically very difficult, and is encompassed in the first two objectives of this paper (see end of section).

As stated earlier, the impact of the jets formed by bubble involution can cause both erosion and acoustic emission, and an association between such jetting and luminescent emission is demonstrated in figures 1 and 2 taken from Dear & Field (1988) and Dear, Field & Walton (1988). Figure 1 shows the collapse of a circular two-dimensional cavity formed in a gel by a shock of strength 0.26 GPa. The shock can be seen encircling the cavity in frame 1. The rear surface of the cavity begins to involute to form a jet in frame 5. The jet crosses the cavity and the gas is compressed into two lobes. Other work (Bourne & Field 1992) has shown that these lobe regions progress as a pair of vortices which travel downstream after the shock. In a three-dimensional cavity, the gas would be compressed into an annulus.

Figure 2 shows a single 3 mm diameter cavity collapsed under similar conditions to those in figure 1 but this time viewed through an image intensifier. The picture shows the time-integrated luminescence from the collapsed cavity. A small amount of background lighting has been added, which reflects off the stationary position of the bubble wall to reveal the circular shape the cavity assumed prior to collapse. There is a bright spot on the side of the cavity where the shock first interacts, but this did not appear in all sequences and is probably an artefact caused by an imperfection in the

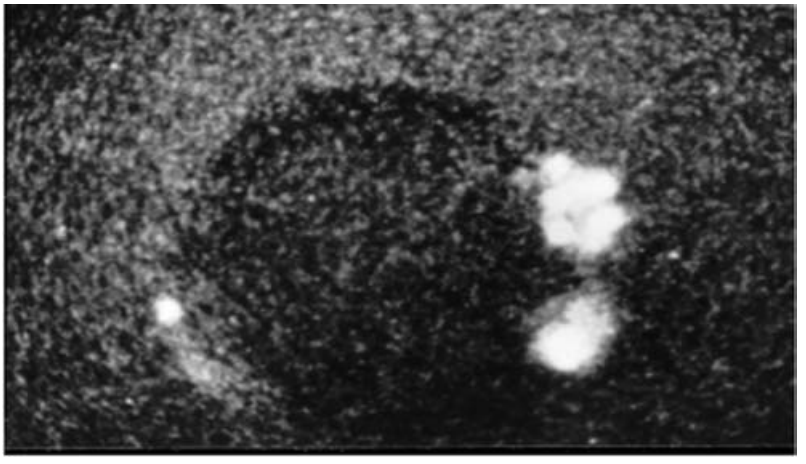

FIGURE 2. A 3 mm diameter cavity before collapse. The shock moved left to right. The luminescence is concentrated in the lobes on either side of the jet. (After Dear *et al.* 1988.)

gel surface. It is clear that most light is produced from the two lobe-shaped regions of trapped gas on either side of the jet. These conform to the shape of the cavity wall during the later stages of collapse (see frame 10 of figure 1).

Measurements of the volume of gas luminescing show that luminescence takes place when the gas volume has been compressed to less than 10% of its initial volume. The luminescence shows a definite structure with some brighter regions, which indicates inhomogeneous conditions. Such inhomogeneities have now been predicted by Ball *et al.* (2000). Clearly, therefore, cavity collapses of sufficient energy to create hot spots and erosion may be associated with luminescence, even though the detailed mechanisms causing luminescence need further research.

Cavitation luminescence is often very faint, being of the order of a few hundred photons $\mathrm{cm}^{-2}\,\mathrm{s}^{-1}$ at the detector, with certain exceptions under very specific conditions (Gaitan *et al.* 1992; Barber *et al.* 1992). As mentioned earlier, van der Meulen had problems with sensitivity and signal-to-noise ratios in his light detection, and could not quantify the emission in absolute terms. Photon counting is deployed in this paper in an attempt to resolve these issues, specifically by achieving four objectives:

(i) detect cavitation luminescence in 'undoped' water as a result of flow over a hydrofoil;

(ii) measure absolute photon count and investigate variation with flow parameters (C_{ref} and cavitation index σ);

(iii) investigate whether there is any departure in the arrival times of the photons from that expected if each time interval has an equal probability of generating/detecting a photon emission (i.e. whether the photons are emitted in 'bursts');

(iv) estimate the limits of the temporal structure in the 'bursts'.

Objective (iii) is designed to investigate whether, as van der Meulen's visual observations suggested, the luminescence occurs in bursts. Objective (iv) aims to put limits on the timescales involved. These two objectives present particular technical difficulties. The first stage of photon counting requires sampling rates of $10^9\,\mathrm{s}^{-1}$ or better, since the individual photon pulses do not exceed nanosecond order. But because hydrodynamic cavitation is a somewhat imprecise phenomenon, sample lengths of duration $O(100\,\mathrm{s})$ are required to investigate the time interval between the 'bursts'

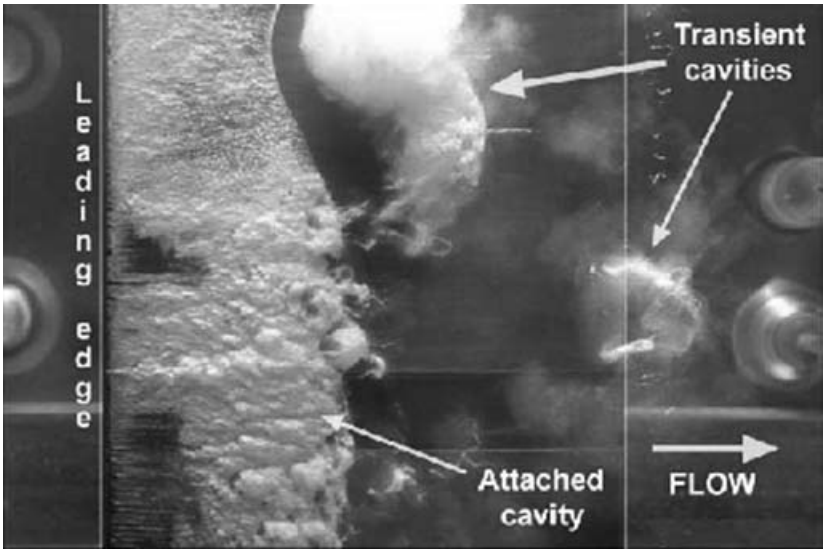

FIGURE 3. Top view of leading-edge cavitation on a NACA 009 two-dimensional hydrofoil of 100 mm truncated chord length. The flow is from the left. $C_{ref} = 30\,\mathrm{m\,s^{-1}}$, $\alpha = 3.5°$, $\sigma = 0.9$.

described by van der Meulen. Few systems can sample real time at $10^9\,\mathrm{s^{-1}}$ for $O(100\,\mathrm{s})$ and in fact the data, from which temporal characteristics were to be inferred, came as accumulated distributions of the number of photons which arrived in (almost) consecutive 20 ms time windows.

These four objectives represent further investigation of the techniques for detecting luminescence from hydrofoil cavitation, rather than investigation of all aspects raised by earlier workers. Interested readers are directed to the conference papers in the reference list which comprise the only previous publications in this field, a dearth which perhaps reflects, in the authors' experience, the greater technical difficulties in measuring this luminescence compared to that associated with acoustic cavitation.

2. Leading-edge cavitation

The generation of transient cavities in leading-edge cavitation flow has been widely investigated. Figure 3 shows a top view of leading-edge cavitation occurring on a two-dimensional hydrofoil in the EPFL high-speed cavitation tunnel for an incidence angle of 4° and an upstream velocity of $30\,\mathrm{m\,s^{-1}}$.

Dupont (1993) investigated the flow field downstream of the main cavity with laser Doppler anemometry and observed an intense shear stress in the vicinity of the main cavity interface. The interaction of the resulting vorticity lines with the Kelvin–Helmholtz instabilities leads to the formation of U-shaped vortices as illustrated in figure 3. These vapour cavities are convected by the mean flow to the pressure recovery region where they collapse. Figure 4 shows schematically the generation and convection mechanisms for the transient cavities.

Farhat, Pereira & Avellan (1993) and Farhat (1994) investigated the shedding process of the transient cavities in leading-edge cavitation flow by measuring the pressure fluctuations induced downstream of the main cavity. They showed that increases of the incidence angle, the upstream velocity, or the cavity length, promote

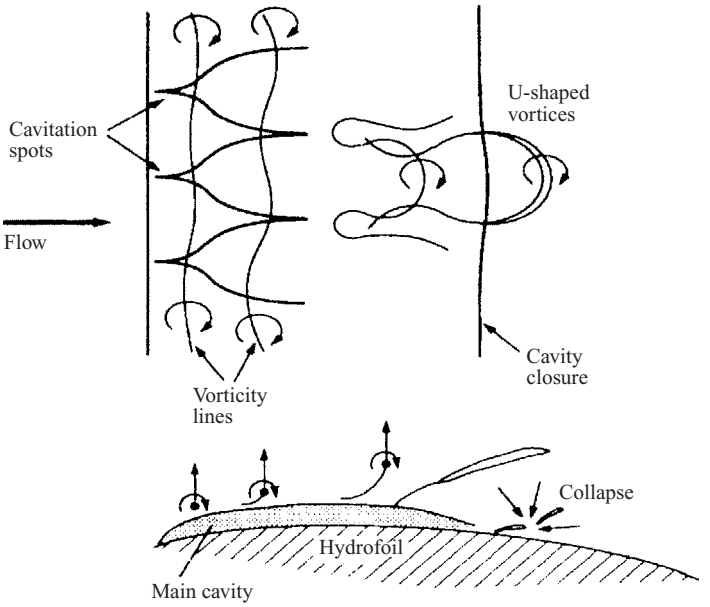

FIGURE 4. Generation mechanism for transient U-shaped vortices in a leading-edge cavitation flow. Aligned top and side view are shown. The arrows denote the directions of vortex rotation and movement away from the hydrofoil. (After Avellan *et al.* 1989.)

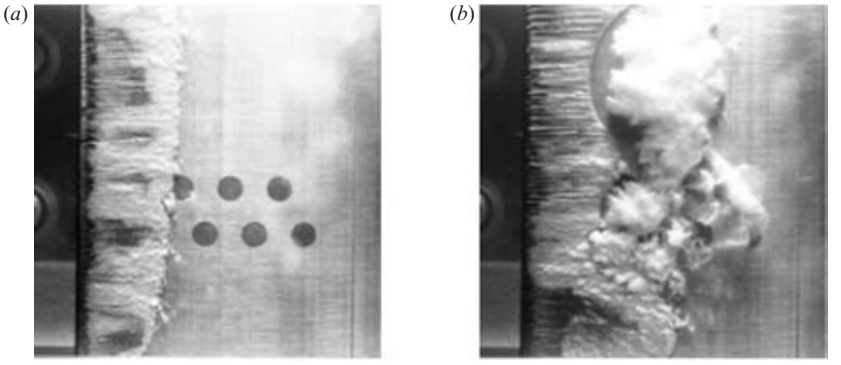

FIGURE 5. Illustration of (*a*) stable: $C_{ref} = 20\,\mathrm{m\,s^{-1}}$, $\alpha = 2.5^\circ$, $\sigma = 0.81$ and (*b*) unstable: $C_{ref} = 35\,\mathrm{m\,s^{-1}}$, $\alpha = 4.5^\circ$, $\sigma = 1.1$ cavitation. The flow is from the left.

instabilities in the main cavity behaviour which strongly influences the shedding process. Figure 5 illustrates the stable and unstable regimes of the main cavity. These photographs were obtained during studies of flow over a two-dimensional hydrofoil in the EPFL high-speed cavitation tunnel.

In the stable regime, the size of transient cavities as well as the amplitude of the main cavity fluctuations are small when compared to the main cavity length, and the shedding process is found to be intermittent (Franc & Michel 1985). When the main cavity is in the unstable regime, the size of transient cavities as well as the amplitude of the main cavity pulsation are of the same order as the main cavity length. In this case, the shedding process is controlled by a Strouhal-type law. The Strouhal number

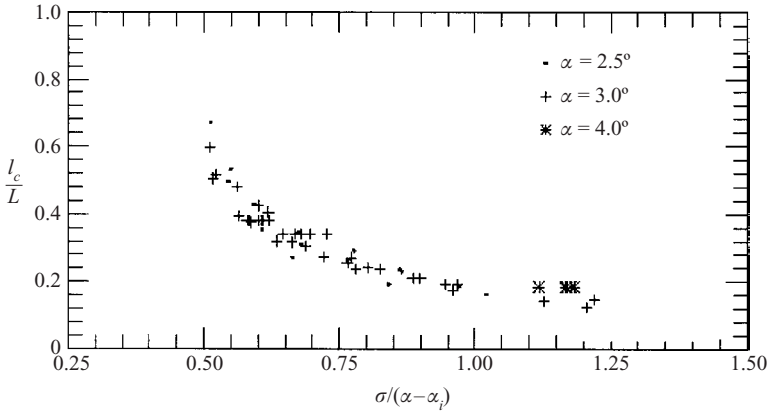

FIGURE 6. Plot of l_c/L versus $\sigma/(\alpha - \alpha_i)$ where α_i is the incident angle. Note the data fall on a 'master' curve. (After Farhat 1994.)

is defined by

$$S = \frac{f_s l_c}{C_{ref}}, \tag{1}$$

where f_s denotes the shedding rate of the transient cavities, l_c is the main cavity length and C_{ref} is the upstream velocity. The Strouhal number depends on the incidence angle and lies between 0.2 and 0.3 for incidence angles α ranging from 2° to 5°, and velocities from 20 to 35 m s^{-1} (Franc & Michel 1985; Dupont 1993; Farhat 1994; Pereira, Avellan & Dupont 1998; Bourdon 2000). These values cover the conditions used in the present study.

It is useful to use σ, the dimensionless cavitation index, which is related to the pressure at the inlet of the test section, p_{ref}, and is defined by

$$\sigma = \frac{p_{ref} - p_v}{\frac{1}{2}\rho C_{ref}^2}, \tag{2}$$

where p_v denotes the vapour pressure and ρ is the liquid density. If the ratio of cavity length/chord length, l_c/L, is plotted against σ for a particular angle α then an L-shaped curve is obtained. For different values of α, a family of curves is generated. Franc & Michel (1985) have shown that if l_c/L is plotted against $\sigma(\alpha - \alpha_i)$ where α_i is the incipient angle for cavitation, then the data all fall on a 'master curve'.

Figure 6, illustrates such a 'master curve' using data obtained in the facility used for the present study (see below) by Farhat (1994). Cavity lengths were measured using laser sheet techniques. The curve of α_i versus σ is given in figure 7. Knowing σ and α, and using figure 7 it is possible to find α_i. This allows $\sigma/(\alpha - \alpha_i)$ to be calculated and l_c to be obtained from figure 6. Values of l_c obtained in this way are given in tables 2 and 3. In some cases, the quantity $\sigma/(\alpha - \alpha_i)$ falls outside the range of the data in figure 6 and l_c cannot be calculated. Finally, the shedding frequency, f_s, is calculated using equation (1) with a value of $S = 0.3$. Values are given in tables 2 and 3.

3. Experiment

The experiments were carried out in the EPFL high-speed cavitation tunnel (Avellan, Henry & Ryhming 1987). The dimensions of the test section are $0.15 \times 0.15 \times 0.75$ m^3. A maximum velocity of 50 m s^{-1} can be reached at the inlet

σ	(i) Total no. photons	(ii) Modal occupancy	(iii) Number of windows	(iv) Upper limit on interburst rate (s^{-1})	(v) Lower limit on intraburst rate (s^{-1})	l_c (mm)	f_s (s^{-1})
0.9	295 000	–	–	–	–	–	–
1.0	290 000	–	–	–	–	–	–
1.1	289 000	–	–	–	–	–	–
1.2	288 000	72 ± 5	4000	19 ± 2	3600 ± 300	30 ± 2	300 ± 50
1.3	285 000	67 ± 6	4254	20 ± 2	3350 ± 300	12 ± 1	750 ± 125
1.4	267 000	63 ± 6	4238	20 ± 2	3150 ± 300	6 ± 0.5	1500 ± 250
1.5	235 000	46 ± 7	5109	24 ± 4	2300 ± 350	–	–

TABLE 2. Data for C_{ref} constant at $30\,m\,s^{-1}$, angle constant at 4°, and σ varying column (iii) is obtained by dividing (i) by (ii), column (iv) by dividing (iii) by the length of the experiment (210 s) and column (v) by dividing (ii) by the window duration (20 ms). See the text for further details.

C_{ref} (m^{-1} s)	(i) Total no. photons	(ii) Modal occupancy	(iii) Number of windows	(iv) Upper limit on interburst rate (s^{-1})	(v) Lower limit on intraburst rate (s^{-1})	f_s (s^{-1})
18.3	118 000	15 ± 5	7867	37.5 ± 13	750 ± 250	150 ± 25
20.0	175 000	28 ± 5	6250	30 ± 5	1400 ± 250	180 ± 30
22.0	215 000	40 ± 5	5375	26 ± 4	2000 ± 250	210 ± 35
24.6	245 000	53 ± 5	4623	22 ± 2	2650 ± 250	215 ± 40
25.8	260 000	62 ± 7	4194	20 ± 2	3100 ± 350	230 ± 40
28.0	280 000	72 ± 7	3888	18.5 ± 2	3600 ± 350	250 ± 40
30.0	280 000	74 ± 3 85 ± 3	–	–	–	–
32.1	310 000	92 ± 10	3370	16 ± 4	4600 ± 500	270 ± 45

TABLE 3. Data for angle constant at 4°, σ constant (~ 1.1) and C_{ref} varying. In all cases, l_c equals 3 mm. See caption to table 2 and text for further details.

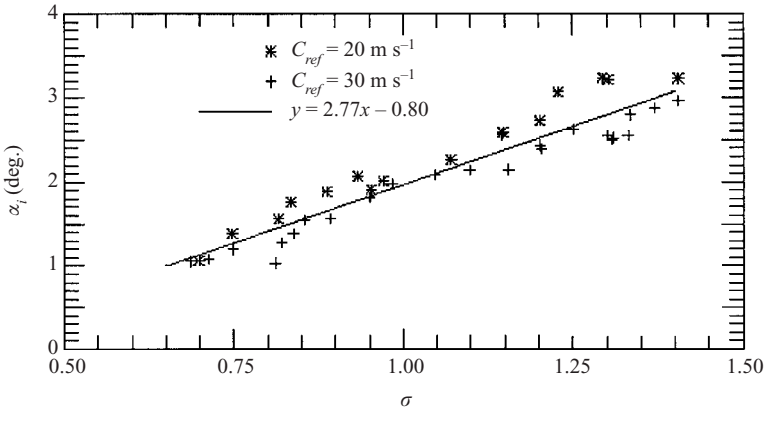

FIGURE 7. Data for α_i versus σ. Use of figures 6 and 7 allows the cavity length to be estimated. (After Farhat 1994.)

of the test section. The experimental hydrofoil was a NACA 009 truncated at 90% of its chord length. The truncated hydrofoil is 100 mm long and 150 mm wide and its maximum thickness is 10 mm. The operating parameters for the cavitation tunnel that were controlled were the upstream velocity at the inlet of the test section C_{ref}, the incidence angle of the hydrofoil, α, and the cavitation index, σ.

Details of the experimental procedure can be found in Leighton *et al.* (2001). As detailed earlier, the first two objectives of the current experiment are to count the photons of cavitation luminescence from flow in a cavitation tunnel, and to determine the dependence of the emission upon the flow parameters. The third objective is to look for any evidence of 'bursts', and the fourth to estimate timescales associated with these, if they are present. To accomplish this, the major problem that had to be overcome was the collection of data over $O(100\,\mathrm{s})$ when the individual photon events were of nanosecond order.

As a system for measuring low levels of light, photon-counting has three advantages over more conventional techniques such as DC current measurement. First, the long-term gain stability is better, the system gain being relatively insensitive to any fluctuations in the high voltage of the detector. Second, the signal-to-noise ratio is optimized. Third, drifts in the zero-offset output (a function of temperature) or DC leakage from the photomultiplier are unable to affect the result. The digital nature of the output is suitable for processing, which in this experiment involved measurement of temporal differences between pulses, and so is sensitive to the presence of noise. The presence of noise photons in the 'quiet' interval between signal photons could contribute spurious high-rate data. It was essential, therefore, to maintain a high signal-to-noise ratio, to take data over a long period and to discriminate pulses, as detailed below.

The use of a lower threshold on its own to remove noise is not appropriate. Whilst this would eliminate the low-amplitude pulses which arise mainly from two sources (spontaneous emission within the photomultiplier, and radio frequency noise), it would not screen out the classes of noise that occur within photomultipliers which have amplitudes greater than the amplitude of pulses resulting from true photon detection. This high-amplitude noise can be due to radioactivity in the proximity of the photomultiplier, or to the Cherenkov photon emissions caused by cosmic ray passage, or by positive ion feedback (where gas molecules within the imperfect vacuum of the photomultiplier become ionized by the electric field, and cause high-energy pulses). To eliminate these noise sources, it is necessary to include an upper threshold in addition to the lower one. The detection of true photons should result in a pulse of energy intermediate between these two thresholds. Noise pulses should ideally lie outside these thresholds. By careful choice of a fast photomultiplier, which in addition emits photon-related pulses within a narrow and well-defined energy range, it is possible to reject both high- and low-amplitude noise pulses by the use of a discriminator.

Photon counting records, in some format, the number of photons detected in a certain time interval. Hence the result depends on the quantum efficiency (QE) of the photomultiplier tube (the probability of a photon ejecting a photoelectron from the photocathode and therefore being recorded as a pulse). The EMI 9789B bialkali tube used here peaks at 30% for light of 380 nm wavelength, falling to 1% at 600 nm (with QE $> 20\%$ between 310 nm and 470 nm).

However, whilst photon counting has the advantages listed above, its use meant that conventional time-histories of luminescence, which would be amenable to standard rate analysis, were not possible. As described at the end of § 1, real-time sorting

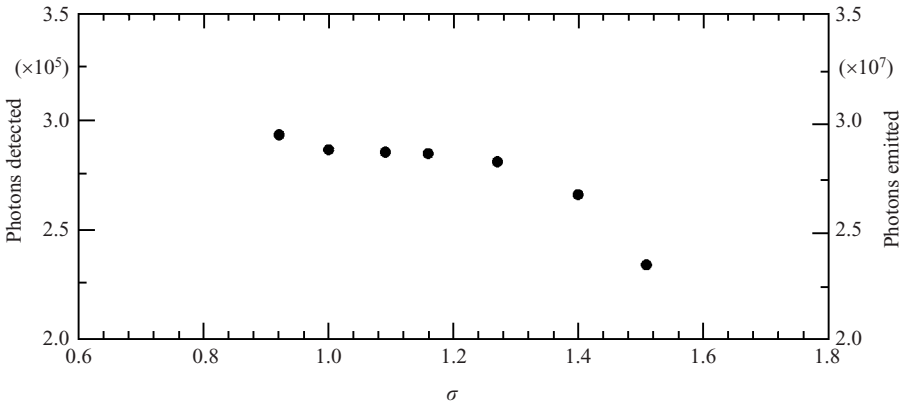

FIGURE 8. Total number of detected photons as a function of cavitation index for $\alpha = 4°$ and $C_{ref} \sim 30\,\mathrm{m\,s^{-1}}$. The right hand axis is the estimated total number of photons emitted (see text).

of these discrete photon detection events is necessary. Therefore the time series data were divided into 20 ms windows, with approximately 1 ms deadtime between windows (note that if two or more photons arrive within any 200 μs interval, then only the first is counted). Each time-history comprised 10 000 windows, having therefore 210 s duration (including an accumulated 10 s of inter-window deadtime). Real-time acquisition of such large amounts of information meant that the data stored were the statistics associated with the window 'occupancy' (number of photons which a given single window contains). The chronology of arrivals could not be stored. From the resulting data-set, the total photon count in the acquisition period could be measured, and plotted as a function of tunnel parameters (upstream flow speed, C_{ref}, incidence angle, α, cavitation number, σ). This would satisfy objectives (i) and (ii).

However, the lack of chronology mean that care had to be taken not to over-analyse the data in achieving objectives (iii) and (iv). If the luminescence emission does contain 'bursts', and if the statistics of their emission is time-invariant, then over a sufficiently long observation time two characteristic timescales in photon arrivals can be defined. The first is the 'interburst rate', the reciprocal of the mean interval between bursts. The second is the 'intraburst rate', the reciprocal of the mean interval between photon arrivals within a given burst. The analysis provides an upper limit on the 'interburst rate', and a lower limit on the 'intraburst rate'. For a fixed value of the interburst rate, the intraburst rate will increase as the total luminescent output increases. The interburst rate will depend on the fluid processes which generate luminescent cavities: for example, if the bulk of the luminescence occurs from shed cavities, then the interburst rate will increase as the shedding rate increases.

4. Results

The photocathode used had an effective diameter of 10 mm and was mounted 160 mm above the blade. Assuming spherical symmetry in the emission, the detector presents an acceptance angle of 3.07×10^{-3} steradian and records approximately 0.0244% of the total luminescence emitted.

Figures 8 and 9 show the total photon count collected into the 3.07×10^{-3} steradian solid angle during the 210 s detection time. Figure 8 shows the count as σ varies, for approximately constant C_{ref} ($30\,\mathrm{m\,s^{-1}}$; values to 3 significant figures given in table 2).

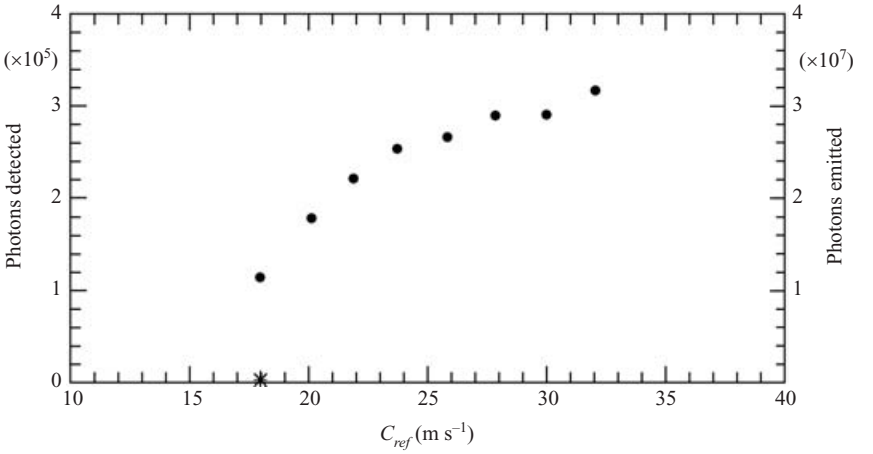

FIGURE 9. Total number of detected photons as a function of flow speed for $\alpha = 4°$ and $\sigma \sim 1.1$. The right hand axis is the estimated total number of photons emitted (see text). The star is for a cavitation-free case.

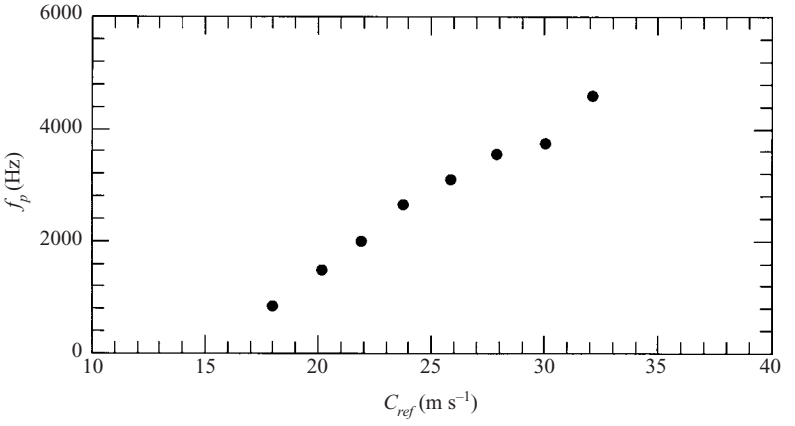

FIGURE 10. Lower limit on intraburst rate, f_p, versus C_{ref} for $\alpha = 4°$, $\sigma \sim 1.1$. Note that this continues to increase approximately linearly.

Figure 9 shows the data for varying C_{ref} and σ held approximately constant (~ 1.1; values to 3 significant figures in table 3). Data on the lower limit of the intraburst rate given in table 3 are plotted in figure 10; note the almost linear relationship. Figure 11 shows, for the parameter sets outlined in table 3, examples of histograms showing the total number of photons in a 210 s data set which occur in windows having a given occupancy (the occupancy of each 20 ms window is the number of photons contained within that window). Such histograms are generated from corresponding histograms of the number of windows that show a given window occupancy (Leighton *et al.* 2001). Unlike figure 11 (which must by definition have a data point at the origin), histograms of this number of windows show a large zero count (i.e. many windows are empty), and if the arrival times of photons were random, would exhibit a Poisson distribution (as they do in the absence of cavitation luminescence – Leighton *et al.* 2001). When cavitation luminescence does occur, most windows still contain no photons, with a Poisson-like tail extending to those windows containing < 10 photons. However there

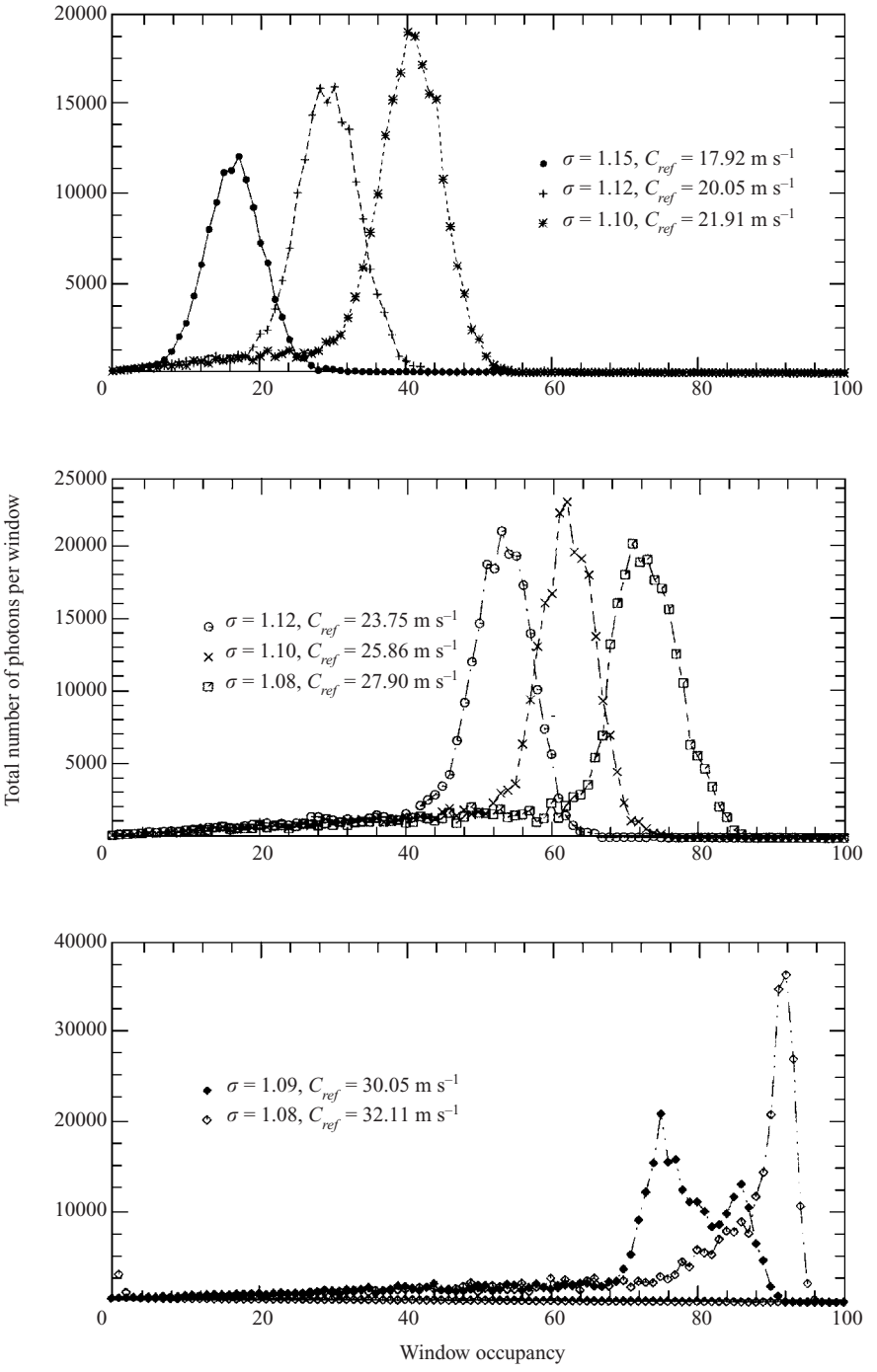

FIGURE 11. Histograms of total number of photons per window occupancy (i.e. the number of photons in a 20 ms window) for increasing flow speed for $\alpha = 4^\circ$ and $\sigma \sim 1.1$. The modal occupancy is given as column (ii) in tables 2 and 3. Integration of the area under these peaks gives the total number of photons.

is, superimposed on this, a peaked distribution. Analysis of all data shows that the mode of this distribution always increases with increasing photon count, and is in the range 40–90 photons per window (Leighton *et al.* 2001).

5. Discussion

The photon count, taken from a solid angle comprising 0.0244% of the global space, is seen to increase with increasing flow velocity and with decreasing cavitation index (figures 8 and 9). Both trends, in C_{ref} and σ, are indicative of increasing cavitation intensity. At the highest level of cavitation, the increase in photon count with increasing C_{ref} does not continue at so great a rate, the fall-off occurring at about $C_{ref} \sim 25\,\mathrm{m\,s^{-1}}$, and indeed ceases to increase significantly with decreasing cavitation index below $\sigma \sim 1.2$. However, as figure 10 shows, the lower limit on the intraburst rate, f_p, continues to increase approximately linearly with increasing C_{ref}.

Note that to convert from the total number detected to the total number emitted per second, the detected number has to be multiplied by 5 (the quantum efficiency is $\sim 20\%$) and divided by 2.44×10^{-4} (fraction of photons intercepted by the detector) and 210 s (length of experiment).

When the cavitation index is decreased, the main cavity closure, from which the transient vortices are generated, moves toward the trailing edge. Furthermore, the cavity dynamics are known to be highly influenced by the flow velocity and the cavitation index for a fixed incidence angle. For a given cavity length, an increase of the flow velocity may promote strong instabilities which lead to a substantial increase of the main volume of the transient cavities. Such instabilities may also be promoted by an increase of the cavity length at a fixed flow velocity. Therefore, the collapse location of the transient cavities moves toward the trailing edge of the blade and may be beyond the field of view of the photomultiplier. Another possibility is that the increased cavitation may prevent luminescence reaching the detector because of optical shielding (as figure 5 illustrates, the air–water interfaces are highly reflective).

Figure 11 shows that, with one exception ($\alpha = 1.09$, $C_{ref} = 30.05\,\mathrm{m\,s^{-1}}$), histograms of the number of photons that occur in windows of a given occupancy exhibit a monomodal distribution. The modal value increases with increasing C_{ref} (figure 10).

The first objective, of obtaining absolute photon counts from this 'undoped' hydrodynamic cavitation, has been achieved, as has the second (figures 8 and 9). The third objective has similarly been accomplished; the departure from the Poisson distribution described at the end of § 4 shows temporal structure in the luminescence. The fourth objective requires setting an upper limit on the interburst rate, and a lower limit on the intraburst rate, for each dataset.

5.1. *The interburst rate*

The value of the interburst rate depends on the organization of the windows of high occupancy. Assume to a first approximation that the data-set contains only windows which are either empty, or are well-populated to a similar extent. If, in a given data-set, all the highly occupied windows occurred in a single cluster, there would be no period to the bursts. The only statement that could be made is that any low-rate structure associated with this data envelope would have a period greater than the duration of the experiment (210 s) and therefore a rate less than $1/210\,\mathrm{s^{-1}}$. At the other extreme, a high value for this interburst rate would occur if the highly occupied windows

occurred singly and evenly spaced. If the windows were evenly spaced, any grouping characteristic between these two limits would give a lower rate than this. Therefore, this estimates the maximum value that the interburst rate component could take if it is assumed that the window groups repeat at one particular fixed rate (i.e. are evenly spaced).

In practice there is a range of window occupancy values clustered about the mode. The highest value that the interburst rate can take is found through finding the number of well-occupied windows through integration of the relevant modal peak of curves of the type shown in figure 11, and assuming that this number of windows is evenly distributed and not adjacent throughout the time series data.

The results of the calculations are shown in table 2 for the data relating to constant C_{ref} and varying σ. Estimates of the number of windows containing many photons (column (iii)) are obtained by dividing the total photon count (column (i), as shown in figure 8) by the modal window occupancy (column (ii) taken from the high-occupancy peak of data). The upper limit for the interburst rate is therefore obtained by dividing the modal number of high-occupancy windows (column (iii)) by the length of the experiment (210 s). This is shown in column (iv). Note that, as expected, estimates associated with the interburst rate are insensitive to the solid angle of the photomultiplier, which divides out in the above calculations.

Similar values can be obtained for the variation of C_{ref} at constant σ (table 3).

5.2. *The intraburst rate*

If the photons within the burst are assumed to be evenly spaced, the minimum value of the intraburst rate which characterizes their emission would simply be the modal window occupancy divided by the window duration (20 ms). Standard error can be associated with each rate, found from the width of the distributions. These are shown in column (v) of tables 2 and 3, and are found by dividing the values in column (ii) by 20 ms.

Note that the intraburst rates so calculated relate to the acquired data, and not to the total cavitation luminescent emission (which they can be scaled to reflect in this experiment by dividing the intraburst rate in the photomultiplier data by 0.0244%, compensating for the solid angle sampling with a first-order spherical approximation).

5.3. *Possibility and effect of undercounting*

With a finite dead-time of 200 μs, a window occupancy of greater than 100 cannot be recorded. However, the more subtle effect of undercounting becomes more likely the greater the window occupancy, leading to underestimates of both the total photon count (figures 8 and 9) and possibly in the modal window occupancy (figure 11). The likelihood of the effect on the rate estimates in tables 2 and 3 can be assessed. Confidence can be placed in rows 1–3 of table 3 ($C_{ref} = 18.3$, 20.0 and 22.4 m s^{-1}), and row 7 of table 2 ($\sigma = 1.5$), where the modal window occupancy is less than 50 photons per 20 ms window (averaging 400 μs between photons), and the effect of undercounting is likely to be small. Only in these rows is the estimate of the minimum value of the high rate less than the 2500 Hz Nyquist frequency. As one moves further down table 3, or up table 2, the possibility increases that both the total number of photons (column (i)) and the modal window occupancy (column (ii)) may include an element of undercounting, and so are underestimates. This would lead to column (v), the lower limit on the intraburst rate, being an overestimate: therefore, the error is

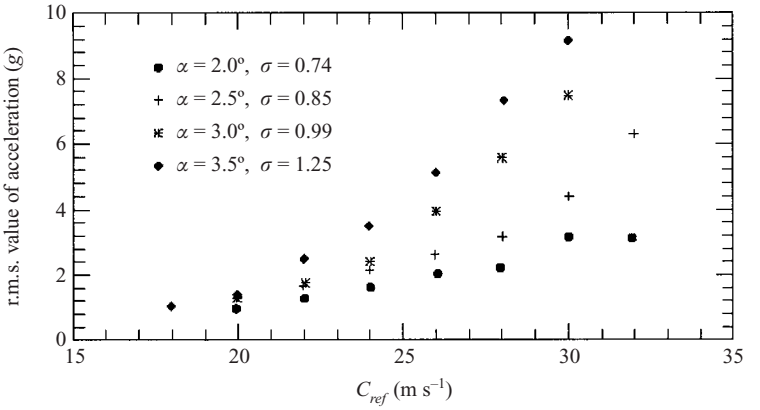

FIGURE 12. The vibration of a NACA 009 blade. The r.m.s. values of acceleration (in units of g) versus C_{ref}. (After Farhat 1994.)

reduced. However, the direction of the error in the estimates in rows 4–8 in column (iv) cannot readily be assessed.

5.4. *Comparison with other parameters*

The relation between the onset of cavitation luminescence and acoustic noise was examined in the work of van der Meulen (1986*b*). In experiments using the EPFL high-speed cavitation tunnel and the NACA 009 blade, Farhat (1994) gives data on the vibration generated for various flow conditions. The recording accelerometer was a Kistler 8614A gauge with a resonant frequency of 125 kHz and a sensitivity of 2.61 mV g^{-1} where g is the acceleration due to gravity. It was mounted in the root of the blade and the signal was integrated between 0 and 100 kHz. The results are reproduced in figure 12, the top curve being the closest to the conditions of the present study. The interesting point is that the onset of significant vibration occurs at similar flow conditions to the luminescence (figures 9 and 10). There is no reason why the curves above the onset velocity should have similar shapes, and, as noted earlier, the plateau achieved in figure 9 may be an artefact caused by the detection of luminescence.

6. Conclusions

The present research has used photon counting to detect luminescence during flow over a blade in a high-speed cavitation tunnel. Earlier research by Dupont (1993), Farhat *et al.* (1993) and Farhat (1994) has recorded and described the build-up of a main cavity and the conditions under which U-shaped vortices (cavities) shed from the main cavity. The conditions under which these cavities collapse and cause erosion are well-established.

The key result of the present research is that significant photon counts are recorded in undoped water when the cavities collapse transiently with the potential to cause erosion. The photon count increases dramatically as the velocity C_{ref} is further increased (see, for example, figure 9) or σ reduced (see figure 8). Eventually the photon count reaches a plateau. This may be due, as noted earlier, to the increased bubble cloud obscuring the source of luminescence or simply the collapse sites moving

to a position partly out of the field of view of the photomultiplier. The more physically significant curve is probably figure 10 which shows that the lower limit estimate of the intraburst rate continues to increase with C_{ref}.

The 'bursts' observed by eye by van der Meulen have been confirmed indirectly, and an upper limit set on the intraburst rate, and a lower limit set on the intraburst rate, for each data-set.

The interburst rate is not necessarily related to the shedding rate f_s in a simple way. The number of vortices which are shed from the main cavity per second may be higher than f_s since they may be shed from multiple points from the rear of the main cavity. This is supported by photographs taken by Dupont (1993). Additionally, there are high-speed photographs (Farhat 1994) showing that a vortex may collapse 2 or 3 times as it progresses along the blade. Alternatively, if not all of the vortices collapsed with sufficient energy to generate luminescence, then the interburst rate could be less than f_s. Using the procedure outlined in § 2, it is possible to estimate f_s from equation (1). Values are given in tables 2 and 3 assuming a Strouhal number $S = 0.3$. Two interesting results emerge from the estimated upper limit on interburst rates. First, they are less than the shedding frequency, f_s, and secondly the rate decreases with increasing C_{ref} (table 3).

Thus whilst the measures of the intensity of cavitation (erosion, vibration, total photon count) tend to increase with increasing C_{ref} or decreasing σ, and whilst the lower limit on the intraburst rate also increases (indicating that the luminescent bursts are tending to become brighter), the upper limit on the interburst frequency decreases. This effect, and the plateauing of the total luminescence (figure 9) may occur for the reasons noted above, namely that the bubble cloud obscures the sources of luminescence or the sources move outside the field of view of the photomultiplier. An alternative explanation is that though there are more collapsing vortices, a small number collapse violently producing luminescence. If this is the case, table 3 suggests that at $C_{ref} = 18.3\,\mathrm{m\,s^{-1}}$ only 1 in 4 collapse violently while at $C_{ref} = 32.1\,\mathrm{m\,s^{-1}}$ the ratio is 1 in 17.

There is a large body of literature on the erosion of materials by cavitation, but most researchers obtain data using an accelerated test (Knapp *et al.* 1970). Obtaining data from a cavitation tunnel is a lengthy process and the approach is usually to detect the onset of pitting, which occurs earlier than measurable weight losses. Couty (2001) has performed such experiments in the IMHEF tunnel and he finds that the onset of pitting in metals such as aluminium 1050 correlates reasonably well with our measurements for the onset of luminescence. The onset of cavitation luminescence, noise, vibration and pitting damage correlate reasonably well, though more research is needed.

In future research, an image intensifier system could be used to give spatial resolution similar to the photographic work of van der Meulen & Nakashim (1983), but with video time resolution. Now that the upper limit on the interburst rate is known, a system could be designed which exploits photomultiplier current to provide a time series suitable for rate analysis. This would allow more detailed research on the shedding and transient collapse processes.

J.E.F. and T.G.L. thank EPFL for the opportunity to bring the Cambridge photon detectors to perform an experiment on the EPFL cavitation tunnel. The research was performed during a series of study leave visits and EPFL, the Royal Society (London), the Swiss National Science Foundation and the Royal Academy of Engineering (London) are thanked for their support.

REFERENCES

Arndt, R. E. A. 2002 Cavitation in vortical flows. *Annu. Rev. Fluid Mech.* **34**, 143–175.

Avellan, F., Dupont, P. & Farhat, M. 1991 Cavitation erosion power. *Proc. "Cavitation 91" Symposium, 1st ASME-JSME Fluid Engineering Conf., Portland* (*Oregon*), *USA*, vol. 116 (ed. H. Kato & O. Furuya), pp. 135–140.

Avellan, F., Dupont, P. & Ryhming, I. L. 1989 Generation mechanisms and dynamics of cavitation vortices downstream of a fixed leading edge cavity. *17th Symp. on Naval Hydrodynamics*, pp. 317–329. National Academy Press, Washington DC.

Avellan, F. & Farhat, M. 1989 Shock pressure generated by cavitation vortex collapse. *Proc. Intl Symp. on Cavitation Noise and Erosion in Fluid System. ASME Winter Annual Meeting, San Francisco* (*USA*). FED-88, pp. 119–125.

Avellan, F., Henry, P. & Ryhming, I. L. 1987 A new high speed tunnel for cavitation studies in hydraulic machinery. *ASME Symposium on Cavitation Research Facilities and Techniques, Boston, USA*, vol. 57, pp. 49–60.

Avellan, F. & Karimi, A. 1987 Dynamics of vortex cavitation involved in the erosion of hydraulic machines. *Proc. 7th Intl Conf. on Erosion by Liquid and Solid Impact, Cambridge, UK* (ed. J. E. Field), pp. 25.1–25.8.

Ball, G. J., Howell, B., Leighton, T. G. & Schofield, M. 2000 Shock-induced collapse of a cylindrical air cavity in water: a Free-Lagrange simulation. *Shock Waves* **10**, 265–276.

Barber, B. P., Hiller, R. A., Arisaka, K., Fetterman, H. & Putterman, S. 1992 Resolving the picosecond characteristics of synchronous sonoluminescence. *J. Acoust. Soc. Am.* **91**, 3061–3063.

Barker, B. P., Hiller, R. A., Lofstedt, R., Putterman, S. J. & Weninger, K. R. 1997 Defining the unknowns of sonoluminescence. *Phys. Rep.* **281**, 66–143.

Blake, J. R. 1999 (Ed.) Acoustic cavitation and sonoluminescence. *Phil. Trans. R. Soc. Lond.* A **357**, 199–369.

Bourdon, P. 2000 Détection vibratoire de l'erosion de cavitation des turbines francis. PhD thesis No. 2295, EPFL, Switzerland.

Bourne, N. K. & Field, J. E. 1992 Shock-induced collapse of single cavities in liquids. *J. Fluid Mech.* **244**, 225–240.

Couty, P. 2001 Physical investigation of cavitation vortex. PhD thesis No. 2463, EPFL, Switzerland.

Dear, J. P. & Field, J. E. 1988 A study of the collapse of arrays of cavities. *J. Fluid Mech.* **190**, 409–425.

Dear, J. P., Field, J. E. & Walton, A. J. 1988 Gas compression and jet formation in cavities collapsed by a shock wave. *Nature* **332**, 505–508.

Dupont, P. 1993 Etude de la dynamique d'un poche de cavitation partielle en vue de la prédiction de l'erosion dans les turbomachines hydrauliques. PhD thesis No. 931, EPFL, Switzerland.

Farhat, M. 1994 Contribution á l'etude de l'erosion de cavitation: mécanismes hydrodynamique et prédiction. PhD thesis No. 1273, EPFL, Lausanne, Switzerland.

Farhat, M., Pereira, F. & Avellan, F. 1993 Cavitation erosion power as a scaling factor for cavitation erosion in hydraulic machines. *Proc. 3rd Intl Symp. on Cavitation Noise and Erosion, New Orleans* (*USA*), ASME, Fed-Vol. 176, pp. 95–104.

Franc, J. P. & Mitchel, J. M. 1985 Attached cavitation and the boundary layer: Experimental investigation and numerical treatment. *J. Fluid Mech.* **154**, 63–90.

Gaitan, D. F., Crum, L. A., Church, C. C. & Roy, R. A. 1992 An experimental investigation of acoustic cavitation and sonoluminescence from a single bubble. *J. Acoust. Soc. Am.* **91**, 3166–3183.

Hammer, D. & Frommhold, L. 2001 Sonoluminescence: How bubbles glow. *J. Mod. Optics* **48**, 239–277.

Jarman, P. 1960 Sonoluminescence: a discussion. *J. Acoust. Soc. Am.* **32**, 1459–1462.

Karimi, A. & Avellan, F. 1986 Comparison of erosion mechanisms in different types of cavitation. *Wear* **113**, 305–322.

Knapp, R. T., Daily, J. W. & Hammett, F. G. 1970 *Cavitation*. McGraw-Hill.

Leighton, T. G. 1993 *The Acoustic Bubble*. Academic.

Leighton, T. G., Cox, B. T. & Phelps, A. D. 2000 The Rayleigh-like collapse of a conical bubble. *J. Acoust. Soc. Am.* **107**, 130–142.

Leighton, T. G., Farhat, M., Field, J. E. & Avellan, F. 2001 Luminescence from hydrodynamic cavitation: Method and preliminary analysis. *ISVR Tech. Rep.* 294. University of Southampton.

Marinesco, M. & Trillat, J. J. 1933 Action des ultrasons sur les plaques photographiques. *C. R. Acad. Sci. Paris* **196**, 858–860.

Matula, T. J. & Roy, R. A. 1997 Comparisons of sonoluminescence from single bubbles and cavitation fields: bridging the gap. *Ultrasonics Sonochem.* **4**, 61–64.

van der Meulen, J. H. J. 1983 The use of luminescence as a measure of hydrodynamic cavitation activity. *ASME Cavitation and Multiphase Flow Forum, Houston*, pp. 51–53.

van der Meulen, J. H. J. 1986*a* On correlating erosion and luminescence from cavitation on a hydrofoil. *Intl Symp. on Propellers and Cavitation, Edinburgh*, pp. 13–19.

van der Meulen, J. H. J. 1986*b* The relation between noise and luminescence from cavitation on a hydrofoil. *Joint ACSE/ASME Conf. on Cavitation in Hydraulic Structures and Turbomachinery, Albuquerque, USA*, FED vol. 25 (ed. R. E. A. Arndt & D. R. Webb), pp. 149–159.

van der Meulen, J. H. J. & Nakashim, Y. 1983 A study of the relationship between type of cavitation erosion and luminescence. *Proc. 2nd Intl Conf. on Cavitation, Edinburgh*, I Mech E (Lond.) pp. 13–19.

Pereira, F., Avellan, F. & Dupont, P. 1998 Prediction of cavitation erosion: an energy approach. *Trans. ASME: J. Fluids Engng* **120**, 719–727.

Peterson, F. B. 1966 Light emission from hydrodynamic cavitation. PhD thesis, Northwestern University, USA.

Peterson, F. B. 1967 Monitoring hydrodynamic cavitation light emission as a means to study cavitation phenomena. *Proc. Symp. on Testing Techniques in Ship Cavitation Research Trondheim, Norway*, vol. 2, pp. 3–17.

Walton, A. J. & Reynolds, G. T. 1984 Sonoluminescence. *Adv. Phys.* **33**, 595–660.